Applied Acoustics 116 (2017) 24–32

Contents lists available at ScienceDirect

Applied Acoustics

journal homepage: www.elsevier.com/locate/apacoust

Spatial time-frequency DOA estimation based on joint diagonalization using Jacobi rotation

Jie Shi, De-Sen Yang, Sheng-Guo Shi, Zhong-rui Zhu *, Bo Hu

Acoustic Science and Technology Laboratory, Harbin Engineering University, Harbin, China
College of Underwater Acoustic Engineering, Harbin Engineering University, Harbin, China

ARTICLE INFO

Article history:
Received 12 November 2015
Received in revised form 2 September 2016
Accepted 6 September 2016
Available online 15 September 2016

2010 MSC:
00-01
99-00

Keywords:
Direction-of-arrival
Spatial time-frequency distributions
Joint diagonalization
Jacobi rotation

ABSTRACT

Direction-of-arrival (DOA) estimation consists of locating closely spaced sources impinging from different directions in the presence of considerable noise or interference. Recently, this problem has been solved using spatial time-frequency distribution (STFD) information that is available in the array signals. In this work, a new joint diagonalization approach based on Jacobi rotation, which can efficiently combine all of the relevant STFD points, is proposed to achieve superior DOA resolutions and suppressed sidelobes in the spatial spectrum. It is discovered that our proposed Jacobi technique leads to a non-orthogonal joint diagonalization structure and can avoid pre-whitening the signal component of the observation. In addition, we further adopt the minimum variance distortionless response (MVDR) processor instead of the MUltiple SIgnal Classification (MUSIC) algorithm to avoid the estimation of the signal subspace and noise subspace in the time-frequency DOA domain. Finally, computer simulations of several frequently encountered types of challenging scenarios (such as low SNR and coherent arrivals) show that significant improvements are achieved by our proposed approach in comparison to the existing techniques.

1. Introduction

Direction-of-arrival (DOA) estimation is an area of active interest with applications in radar, sonar, wireless communications, navigation, biomedical systems, and other fields [1]. It is motivated by practical scenarios that involve several source signals and a series of sensors. Each sensor receives a linear mixture of the source signals. Then an important goal for DOA estimation is to locate closely spaced sources impinging from different directions in the presence of considerable noise or interference [2].

During the last half-century, many important milestones in DOA estimation have been achieved. Conventional beamforming (CBF) was the earliest approach for direction-finding in the array signal-processing domain. However, its performance, in particular, suffers from the Rayleigh resolution limit of the physical size of the array (the aperture). Since then, other advanced techniques or criteria (such as the maximum entropy (ME) method, the maximum likelihood (ML) method, and the subspace approach) have been used by various researchers and proven to be effective means for DOA estimation in sensor arrays [3–6]. However, it is noted that the problem of DOA estimation has been solved only by space-time statistical information available on the array signals and not by exploiting the difference in the time-frequency signatures of the sources. This can be done by resorting to the time-frequency (TF) analysis, which is a powerful tool for nonstationary signal representation [7].

TF analysis, or the TF transform, can be viewed as a time-dependent extension of classical Fourier transform methods and has been the subject of many thorough investigations over the past 30 years, culminating in today's classical approaches, such as short-time Fourier transforms (STFT), wavelets, or Wigner-type energy distributions [8]. The underlying motivation generally lies in attempting to understand the time-varying structure of many signals that we encounter, as well as to enable manipulation of these signals in a proper domain that is better suited to their nature of nonstationarity [9]. With the rapid development of methodologies and theoretical approaches for nonstationary signal representations, TF analysis has become an exciting field that has attracted considerable attention in almost all branches of science and engineering such as audio synthesis, medical imaging reconstruction, wavelet denoising, and physiological signal analysis [10]. Moreover, the broad applicability of TF analysis has already inspired notable investigation in the context of array processing [11].

* Corresponding author at: Acoustic Science and Technology Laboratory, Harbin Engineering University, Harbin, China.
E-mail address: shijie@hrbeu.edu.cn (Z.-r. Zhu).

http://dx.doi.org/10.1016/j.apacoust.2016.09.008
0003-682X/

By turning to the TF analysis framework, the underlying problem can then be posed as a signal synthesis from the time-frequency plane with the incorporation of the spatial information provided by the multisensor array [12]. We are then able to exploit the inherent space-time-frequency characteristics of the underlying array signal to achieve better performance even in a noisy and coherent environment with few snapshots [13]. Belouchrani and Amin defined the notion of a spatial time-frequency distribution (STFD) and used the diagonalization of a combined set of STFD matrices to solve the problem of blind source separation for nonstationary signals [7]. After that, they further applied the STFD concept to DOA estimation and introduced a new method for the estimation of the signal subspace and noise subspace based on time-frequency signal representations, named "Time-Frequency Music" [14]. Gershman et al. then extended the narrowband STFD approach to the wideband case and exploited the conventional CSS approach to develop a more general wideband direction-finding method [15,16]. At the same time, Zhang et al. examined the eigenstructure of the STFD matrices and provided statistical analysis of their respective signal and noise subspaces [17]. More recently, Ghofrani developed a high-resolution DOA estimation approach for nonstationary narrowband signals using matching pursuit (MP), which is used to implement the modified STFD based on a Wigner-Ville distribution [18,19]. Sharif et al. provided an influence function robustness analysis of STFD estimators which gives practitioners a simple way to pre-select STFD estimators for their scenarios [20]. In addition, they also considered the problem of estimating STFD matrices in the presence of impulsive noise and proposed robust techniques for STFD estimation [21]. Khodja et al. conducted a performance analysis of the time-frequency MUSIC algorithm in the presence of both additive noise and array calibration errors [22].

Furthermore, STFD has been applied to ocean acoustics. Mansour et al. designed a signal pre-processor dedicated to passive acoustic tomography based on STFD, which is adapted with wide-band transient signals, such as marine mammal vocalizations [23]. In addition, Sabra and Anderson proposed the formation of a generalized STFD matrix from the single-snapshot data by computing Cohen's class time-frequency distributions between all sensor data pairs. This approach is especially suited to handling nonstationary echoes of underwater target resonances that are highly localized in the time-frequency domain [24,25].

Prior research has established STFD as a valuable tool for array signal processing but mainly from a theoretical point of view, seldom considering how to efficiently combine all of the relevant STFD points with stability and convergence concerns, and its application to DOA estimation has been developed only for very limited scenarios. The motivation of this paper is to achieve superior DOA resolutions and suppressed sidelobes in the spatial spectrum by introducing a new joint diagonalization approach based on Jacobi rotations. Different from the work of Belouchrani and Amin [7], our proposed Jacobi technique leads to a non-orthogonal joint diagonalization structure and can avoid pre-whitening the signal component of the observation. Different from the work of Gershman et al. [14–16], our work adopts the minimum variance distortionless response (MVDR) processor, rather than the MUltiple SIgnal Classification (MUSIC) algorithm, to avoid the estimation of the signal subspace and noise subspace. The main contributions of the paper are stated as follows: (1) to the best of our knowledge, this is the first study in which the joint diagonalization approach based on Jacobi rotations is introduced to efficiently combine all of the relevant STFD points; (2) moreover, it is also the first research in which the MVDR processor is adopted instead of MUSIC to avoid the signal subspace and noise subspace estimation in the time-frequency DOA domain.

The remainder of the article is organized as follows. Section 2 presents the array signal model and conventional DOA estimation methods. In Section 3, the STFD-based DOA estimation algorithms are investigated, and a new formulation based on joint diagonalization using Jacobi rotation is described. Section 4 analyzes the numerical results in detail using synthetic data. Finally, the conclusions are summarized in Section 5.

2. Array signal model and conventional DOA estimation

In this section, we review the basic concepts and definitions of the array signal model and conventional DOA estimation methods.

For simplicity, we describe the prevailing narrowband array signal model in the far field of a uniform linear array that is used in the remainder of this article. Let the uniform linear array in consideration consist of N omni-directional sensors with equal spacing d, residing on the horizontal axis as shown in Fig. 1. Consider K narrowband signals $s_k(t)$, $k = 1,\ldots,K$, impinging on the array by incidence angles $\theta_k, k = 1,\ldots,K$, and their corresponding steering vectors are $a(\theta_k) = \left[1, e^{j2\pi f_k d\sin(\theta_k)/c},\ldots, e^{j2\pi f_k (N-1)d\sin(\theta_k)/c}\right]^{\mathrm{T}}, k = 1,\ldots, K$, where f_k denotes the frequency of the k-th narrowband signal, c is the signal propagation speed, and $(\cdot)^{\mathrm{T}}$ denotes the transpose.

Given that the measurement of the array output is corrupted by additive noise, the array output $\mathbf{X}(t)$ can be expressed as

$$\mathbf{X}(t) = \mathbf{A}(\theta)\mathbf{S}(t) + \mathbf{N}(t) \tag{1}$$

where

$\mathbf{X}(t) = [x_1(t), x_2(t),\ldots, x_N(t)]^{\mathrm{T}}$ denotes the sensor outputs;
$\mathbf{A}(\theta) = [\mathbf{a}(\theta_1), \mathbf{a}(\theta_2),\ldots, \mathbf{a}(\theta_K)]$ is called the array manifold matrix;
$\mathbf{S}(t) = [s_1(t), s_2(t),\ldots, s_K(t)]^{\mathrm{T}}$ represents the signal field;
$\mathbf{N}(t) = [n_1(t), n_2(t),\ldots, n_N(t)]^{\mathrm{T}}$ represents the noise field.

The data covariance matrix, commonly used in array signal processing, is defined by

$$\mathbf{R_{XX}} = \mathrm{E}[\mathbf{X}(t)\mathbf{X}^{\mathrm{H}}(t)] \tag{2}$$

where $\mathrm{E}(\cdot)$ is the statistical expectation operator and $(\cdot)^{\mathrm{H}}$ denotes the conjugate transpose.

Further assume that $\mathbf{N}(t)$ is modeled generally as stationary, temporally and spatially white, a zero mean random process, and independent of the source signal $\mathbf{S}(t)$. Then, the data covariance matrix $\mathbf{R_{XX}}$ has the structure

$$\mathbf{R_{XX}} = \mathbf{A}(\theta)\mathbf{R_{SS}}\mathbf{A}^{\mathrm{H}}(\theta) + \sigma\mathbf{I} \tag{3}$$

where $\mathbf{R_{SS}} = \mathrm{E}[\mathbf{S}(t)\mathbf{S}^{\mathrm{H}}(t)]$ is the source covariance matrix, σ is the noise power at each sensor, and $\mathbf{I}$ denotes the identity matrix.

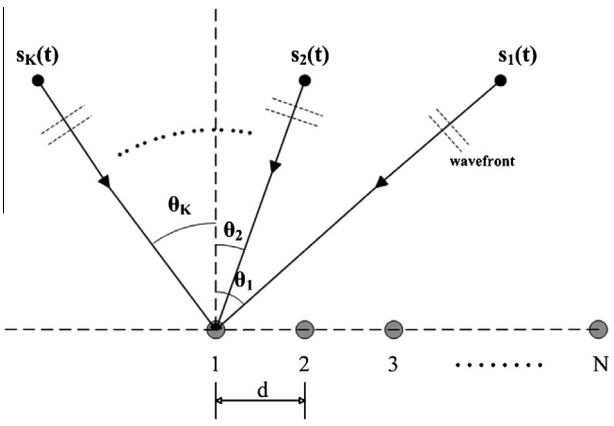

Fig. 1. Array signal model.

In practice, $\mathbf{R_{XX}}$ is unknown and therefore should be estimated from the available Ldata samples (snapshots) $\mathbf{X}(l)$ $(l = 1, 2, \ldots, L)$

$$\widehat{\mathbf{R}}_{\mathbf{XX}} = (1/L)\sum_{l=1}^{L}\mathbf{X}(l)\mathbf{X}^{\mathrm{H}}(l) \tag{4}$$

Almost all of the conventional DOA estimation methods solve the direction-finding problems using the estimated data covariance matrix $\widehat{\mathbf{R}}_{\mathbf{XX}}$, such as CBF, MUSIC, and MVDR.

CBF is a natural extension of classical Fourier-based spectral analysis of sensor array data. This algorithm maximizes the power of the beamforming output for a given input signal and can be formulated as

$$\mathrm{P}_{\mathrm{BF}}(\theta) = \frac{\mathbf{a}^{\mathrm{H}}(\theta)\widehat{\mathbf{R}}_{\mathbf{XX}}\mathbf{a}(\theta)}{\mathbf{a}^{\mathrm{H}}(\theta)\mathbf{a}(\theta)} \tag{5}$$

MVDR attempts to minimize the power contributed by noise and by any signals coming from directions other than θ while maintaining a fixed gain in the "look direction" θ. It can be viewed as a sharp spatial bandpass filter, and its corresponding spatial spectrum can be represented as [26]

$$\mathrm{P}_{\mathrm{MVDR}}(\theta) = \frac{1}{\mathbf{a}^{\mathrm{H}}(\theta)\widehat{\mathbf{R}}_{\mathbf{XX}}^{-1}\mathbf{a}(\theta)} \tag{6}$$

3. STFD-based DOA estimation algorithms

In this section, we first give a brief summary of the STFD structure and the corresponding DOA estimation methods, and we then apply the joint diagonalization technique based on Jacobi rotation for more accurate DOA estimation.

3.1. STFD structure and DOA estimation

The concept of STFDs has been introduced by [7], and its applications to blind source separation and direction-finding have been discussed in [27]. According to [9], the discrete time form of Cohens class of TFDs is given by

$$\mathrm{D}_{xx}(t,f) = \sum_{l=-\infty}^{\infty}\sum_{m=-\infty}^{\infty}\phi(m,l)x(t+m+l)x^{*}(t+m-l)e^{-j4\pi fl} \tag{7}$$

where $(\cdot)^{*}$ denotes the complex conjugate and $t$and $f$respectively represent the time index and the frequency index. $\phi(m,l)$ is the kernel of the TFDs, which characterizes the distribution and is a function of both the time and lag variables.

Similarly, the cross-TFD of two different signals $x_1(t)$ and $x_2(t)$ is represented by

$$\mathrm{D}_{x_1x_2}(t,f) = \sum_{l=-\infty}^{\infty}\sum_{m=-\infty}^{\infty}\phi(m,l)x_1(t+m+l)x_2^{*}(t+m-l)e^{-j4\pi fl} \tag{8}$$

Under the array signal model as shown in Section 2, the STFD matrix can be defined as

$$\mathbf{D}_{\mathbf{XX}}(t,f) = \sum_{l=-\infty}^{\infty}\sum_{m=-\infty}^{\infty}\phi(m,l)\mathbf{X}(t+m+l)\mathbf{X}^{*}(t+m-l)e^{-j4\pi fl} \tag{9}$$

For simplification, assuming a noise-free environment and substituting (1) into (9) yields

$$\mathbf{D}_{\mathbf{XX}}(t,f) = \mathbf{A}(\theta)\mathbf{D}_{\mathbf{SS}}(t,f)\mathbf{A}^{\mathrm{H}}(\theta) \tag{10}$$

where $\mathbf{D}_{\mathbf{SS}}(t,f)$ denotes the source STFD matrix. This representation will be extensively used in the description and implementation of the STFDs-based estimation algorithms.

Note that Eq. (10) is similar to Eq. (3), and that the data covariance matrix $\mathbf{R_{XX}}$, commonly used in conventional array signal processing, can be replaced by the STFDs matrix $\mathbf{D}_{\mathbf{XX}}(t,f)$. Therefore, the algorithms so formed are called STFD-based DOA estimation algorithms. STFD-based methods can handle signals corrupted by interference occupying the same frequency band and/or the same time segment but with different T-F signatures, improving signal selectivity over approaches using the covariance matrix. In addition, the effect of spreading the noise power while localizing the source signal power in the T-F plane increases the effective SNR and provides robustness with respect to noise [27].

According to the above discussion, we can directly introduce the CBF processor and the MVDR processor into the STFD-based methods, and then the following STFD-based CBF and MVDR formulations are, respectively, obtained

$$\mathrm{P}_{\mathrm{BF}}^{\mathrm{TF}}(\theta) = \frac{\mathbf{a}^{\mathrm{H}}(\theta)\mathbf{D}_{\mathbf{XX}}(t,f)\mathbf{a}(\theta)}{\mathbf{a}^{\mathrm{H}}(\theta)\mathbf{a}(\theta)} \tag{11}$$

$$\mathrm{P}_{\mathrm{MVDR}}^{\mathrm{TF}}(\theta) = \frac{1}{\mathbf{a}^{\mathrm{H}}(\theta)\mathbf{D}_{\mathbf{XX}}^{-1}(t,f)\mathbf{a}(\theta)} \tag{12}$$

The superscript $(\cdot)^{\mathrm{TF}}$ indicates that the algorithm is based on the STFD matrix in the time-frequency domain, which is, of course, the function of t and f.

It is important to note that Eq. (10) only utilizes one time-frequency point (t,f). To combine all of the relevant STFD points $(t_k,f_k), k = 1, 2, \ldots, K$, the joint diagonalization based on the Jacobi rotation technique is proposed.

3.2. Joint diagonalization using Jacobi rotation

As stated above, it is necessary to first consider the definition of joint diagonalization: there exists a set of Kcomplex matrices $\mathbf{\Phi} = \{\mathbf{\Phi}_1, \mathbf{\Phi}_2, \ldots, \mathbf{\Phi}_K\}(\mathbf{\Phi}_i \in \mathbf{C}^{N\times N}, i = 1, 2, \ldots, K)$, and it is hoped to find a unitary matrix $\mathbf{U} \in \mathbf{C}^{N\times N}$ and a set of Kcorresponding diagonal matrices $\mathbf{\Lambda} = \{\mathbf{\Lambda}_1, \mathbf{\Lambda}_2, \ldots, \mathbf{\Lambda}_K\}$ such that the following quadratic cost function is minimized:

$$J(\mathbf{U}, \mathbf{\Lambda}_1, \mathbf{\Lambda}_2, \ldots, \mathbf{\Lambda}_K) = \sum_{k=1}^{K}\|\mathbf{\Phi}_k - \mathbf{U}\mathbf{\Lambda}_k\mathbf{U}^{\mathrm{H}}\|_{\mathrm{F}}^2 \tag{13}$$

where $\mathbf{U}$ is called the joint diagonalizer [28].

Now consider the joint diagonalization structure formed by all of the relevant STFD points $(t_k,f_k), k = 1, 2, \ldots, K$, corresponding to Eq. (10)

$$\mathbf{D}_{\mathbf{XX}}(t_k,f_k) = \mathbf{A}(\theta)\mathbf{D}_{\mathbf{SS}}(t_k,f_k)\mathbf{A}^{\mathrm{H}}(\theta) \tag{14}$$

According to the definition of joint diagonalization, Eq. (13) can be converted into an optimization problem that attempts to minimize the following objective function [29]

$$J(\mathbf{A}(\theta), \{\mathbf{D}_{\mathbf{SS}}(t_k,f_k)|k = 1, 2, \ldots, K\}) = \sum_{k=1}^{K}\|\mathbf{D}_{\mathbf{SS}}(t_k,f_k) - \mathbf{A}^{\mathrm{H}}(\theta)\mathbf{D}_{\mathbf{XX}}(t_k,f_k)\mathbf{A}(\theta)\|_{\mathrm{F}}^2 \tag{15}$$

In addition, for the convenience of the following discussion, the entries in $\mathbf{D}_{\mathbf{XX}}(t_k,f_k)$ are denoted as the symbol a, and the entries in $\mathbf{D}_{\mathbf{SS}}(t_k,f_k)$ are denoted as the symbol b.

In numerical analysis, the "off function" of an $n \times n$ matrix $\mathbf{M}$ is defined as

$$\mathrm{off}(\mathbf{M}) = \sum_{i=1,i\neq j}^{n}\sum_{j=1}^{n}|\mathbf{M}_{ij}|^2 \tag{16}$$

where $\mathbf{M}_{ij}$ denotes the (i,j)-th entry of matrix $\mathbf{M}$. Using the "off function", Eq. (15) can be equivalently written as

$$J(\mathbf{A}(\theta)) = \sum_{k=1}^{K} \mathrm{off}(\mathbf{A}^{\mathrm{H}}(\theta)\mathbf{D}_{\mathbf{XX}}(t_k,f_k)\mathbf{A}(\theta)) \tag{17}$$

Thus, the joint diagonalization problem can be represented as the following optimization problem

$$\begin{cases} \min \quad \sum_{k=1}^{K} \mathrm{off}(\mathbf{A}^{\mathrm{H}}(\theta)\mathbf{D}_{\mathbf{XX}}(t_k,f_k)\mathbf{A}(\theta)) \\ \text{s.t.} \quad \mathbf{A}^{\mathrm{H}}(\theta)\mathbf{A}(\theta) = \mathbf{A}(\theta)\mathbf{A}^{\mathrm{H}}(\theta) = \mathbf{I} \end{cases} \tag{18}$$

Generally speaking, the idea behind Jacobi's method is to systematically reduce the "off function". The tools for doing this are rotations of the form

$$\mathbf{g}(i,j,\theta,\phi) = \begin{array}{c} \\ \\ \\ \\ \\ \\ \\ \end{array} \begin{array}{c} \begin{array}{ccccccc} 1 & \cdots & 0 & \cdots & 0 & \cdots & 0 \end{array} \\ \begin{array}{ccccccc} \vdots & \ddots & \vdots & \ddots & \vdots & \ddots & \vdots \end{array} \\ \begin{array}{ccccccc} 0 & \cdots & \cos\theta & \cdots & e^{j\phi}\sin\theta & \cdots & 0 \end{array} \quad i \\ \begin{array}{ccccccc} \vdots & \ddots & \vdots & \ddots & \vdots & \ddots & \vdots \end{array} \\ \begin{array}{ccccccc} 0 & \cdots & -e^{j\phi}\sin\theta & \cdots & \cos\theta & \cdots & 0 \end{array} \quad j \\ \begin{array}{ccccccc} \vdots & \ddots & \vdots & \ddots & \vdots & \ddots & \vdots \end{array} \\ \begin{array}{ccccccc} 0 & \cdots & 0 & \cdots & 0 & \cdots & 1 \end{array} \\ \begin{array}{ccccccc} & & i & & j & & \end{array} \end{array} \tag{19}$$

Eq. (19) is called the complex Jacobi rotations technique, which was originally proposed for diagonalizing a unique Hermitian matrix and now can be extended for the joint approximate diagonalization of a set of normal matrices. Therefore, the joint diagonalization problem of Eq. (18) is finally transformed into a set of successive Jacobi rotations, and $\mathbf{A}(\theta)$ can be represented by the product of the successive Jacobi rotations [30].

In summary, the Jacobi rotation technique involves three basic steps [31]:

(1) choosing an index pair (i,j) that satisfies $1 \leqslant i \leqslant j \leqslant n$;
(2) computing a complex cosine-sine matrix $\mathbf{g} = \begin{bmatrix} \cos\theta & e^{j\phi}\sin\theta \\ -e^{j\phi}\sin\theta & \cos\theta \end{bmatrix}$ such that

$$\begin{bmatrix} b_{ii} & b_{ij} \\ b_{ji} & b_{jj} \end{bmatrix} = \begin{bmatrix} \cos\theta & e^{j\phi}\sin\theta \\ -e^{j\phi}\sin\theta & \cos\theta \end{bmatrix}^{\mathrm{T}} \begin{bmatrix} a_{ii} & a_{ij} \\ a_{ji} & a_{jj} \end{bmatrix} \begin{bmatrix} \cos\theta & e^{j\phi}\sin\theta \\ -e^{j\phi}\sin\theta & \cos\theta \end{bmatrix} \tag{20}$$

is diagonal (as stated before, the symbol *a*and *b*respectively represent the entry in $\mathbf{D}_{\mathbf{XX}}(t_k,f_k)$ and $\mathbf{D}_{\mathbf{SS}}(t_k,f_k)$);
(3) and overwriting $\mathbf{A}$ with $\mathbf{B} = \mathbf{g}^{\mathrm{T}}\mathbf{A}\mathbf{g}$, noting that the matrix $\mathbf{B}$ agrees with $\mathbf{A}$ except in the rows and columns *i*and *j*.

Concretely, the chosen matrix from $\mathbf{D}_{\mathbf{XX}}(t_k,f_k)$ and $\mathbf{D}_{\mathbf{SS}}(t_k,f_k)$ corresponding to the index pair (i,j) can be represented as $\mathbf{D}_{\mathbf{XX}}(t_k,f_k)^{(i,j)}$ and $\mathbf{D}_{\mathbf{SS}}(t_k,f_k)^{(i,j)}$:

$$\mathbf{D}_{\mathbf{XX}}(t_k,f_k)^{(i,j)} = \begin{array}{c} \\ \\ \\ \\ \\ \\ \\ \end{array} \begin{array}{c} \begin{array}{ccccccc} 1 & \cdots & 0 & \cdots & 0 & \cdots & 0 \end{array} \\ \begin{array}{ccccccc} \vdots & \ddots & \vdots & \ddots & \vdots & \ddots & \vdots \end{array} \\ \begin{array}{ccccccc} 0 & \cdots & a_k^{(ii)} & \cdots & a_k^{(ij)} & \cdots & 0 \end{array} \quad i \\ \begin{array}{ccccccc} \vdots & \ddots & \vdots & \ddots & \vdots & \ddots & \vdots \end{array} \\ \begin{array}{ccccccc} 0 & \cdots & a_k^{(ji)} & \cdots & a_k^{(jj)} & \cdots & 0 \end{array} \quad j \\ \begin{array}{ccccccc} \vdots & \ddots & \vdots & \ddots & \vdots & \ddots & \vdots \end{array} \\ \begin{array}{ccccccc} 0 & \cdots & 0 & \cdots & 0 & \cdots & 1 \end{array} \\ \begin{array}{ccccccc} & & i & & j & & \end{array} \end{array} \tag{21}$$

$$\mathbf{D}_{\mathbf{SS}}(t_k,f_k)^{(i,j)} = \begin{array}{c} \\ \\ \\ \\ \\ \\ \\ \end{array} \begin{array}{c} \begin{array}{ccccccc} 1 & \cdots & 0 & \cdots & 0 & \cdots & 0 \end{array} \\ \begin{array}{ccccccc} \vdots & \ddots & \vdots & \ddots & \vdots & \ddots & \vdots \end{array} \\ \begin{array}{ccccccc} 0 & \cdots & b_k^{(ii)} & \cdots & b_k^{(ij)} & \cdots & 0 \end{array} \quad i \\ \begin{array}{ccccccc} \vdots & \ddots & \vdots & \ddots & \vdots & \ddots & \vdots \end{array} \\ \begin{array}{ccccccc} 0 & \cdots & b_k^{(ji)} & \cdots & b_k^{(jj)} & \cdots & 0 \end{array} \quad j \\ \begin{array}{ccccccc} \vdots & \ddots & \vdots & \ddots & \vdots & \ddots & \vdots \end{array} \\ \begin{array}{ccccccc} 0 & \cdots & 0 & \cdots & 0 & \cdots & 1 \end{array} \\ \begin{array}{ccccccc} & & i & & j & & \end{array} \end{array} \tag{22}$$

where $a_k^{(ij)}$ and $b_k^{(ij)}$ respectively denote the (i,j)-th entry of marix $\mathbf{D}_{\mathbf{XX}}(t_k,f_k)^{(i,j)}$ and $\mathbf{D}_{\mathbf{SS}}(t_k,f_k)^{(i,j)}$

Therefore, the optimization problem in Eq. (18) amounts to finding θ and ϕ such that [32]

$$\max \sum_{k=1}^{K} \left(\left(b_k^{(ii)}\right)^2 + \left(b_k^{(jj)}\right)^2 \right) \tag{23}$$

Because $2(|b_k^{(ii)}|^2 + |b_k^{(jj)}|^2) = |b_k^{(ii)} - b_k^{(jj)}|^2 + |b_k^{(ii)} + b_k^{(jj)}|^2$ and the trace $b_k^{(ii)} + b_k^{(jj)}$ is invariant in a unitary transformation, Eq. (23) can be converted into the following form

$$\max(Q = \sum_{k=1}^{K} |b_k^{(ii)} - b_k^{(jj)}|^2) \tag{24}$$

Let

$$\mathbf{u} = \left[b_1^{(ii)} - b_1^{(jj)}, \ldots, b_k^{(ii)} - b_k^{(jj)}, \ldots, b_K^{(ii)} - b_K^{(jj)} \right]^{\mathrm{T}} \tag{25}$$

$$\mathbf{v} = [\cos 2\theta, -\sin 2\theta\cos\phi, -\sin 2\theta\sin\phi] \tag{26}$$

$$\mathbf{g}_k = \left[a_k^{(ii)} - a_k^{(jj)}, a_k^{(ij)} + a_k^{(ji)}, j(a_k^{(ji)} - a_k^{(ij)}) \right]^{\mathrm{T}} \tag{27}$$

then $\mathbf{u}_k = \mathbf{v} \cdot \mathbf{g}_k$, that is

$$\begin{aligned} b_k^{(ii)} - b_k^{(jj)} = {} & (a_k^{(ii)} - a_k^{(jj)})\cos 2\theta - (a_k^{(ij)} + a_k^{(ji)})\sin 2\theta\cos\phi \\ & - j(a_k^{(ji)} - a_k^{(ij)})\sin 2\theta\sin\phi \end{aligned} \tag{28}$$

Thus, the objective function in (24) can be further represented as

$$Q = \sum_{k=1}^{K} |b_k^{(ii)} - b_k^{(jj)}|^2 = \sum_{k=1}^{K} \mathbf{v}^{\mathrm{T}}\mathbf{g}_k\mathbf{g}_k^{\mathrm{H}}\mathbf{v} = \mathbf{v}^{\mathrm{T}}\mathbf{G}\mathbf{G}^{\mathrm{H}}\mathbf{v} \tag{29}$$

where $\mathbf{G} = [\mathbf{g}_1, \ldots, \mathbf{g}_k, \ldots, \mathbf{g}_K]$ is a $3 \times K$-dimension matrix and $\mathbf{v}^{\mathrm{T}}\mathbf{v} = 1$, so

$$Q = \frac{\mathbf{v}^{\mathrm{T}}\mathrm{Re}(\mathbf{G}\mathbf{G}^{\mathrm{H}})\mathbf{v}}{\mathbf{v}^{\mathrm{T}}\mathbf{v}} \tag{30}$$

When $\mathbf{v}$ is the eigenvector corresponding to the maximum eigenvalue of the matrix $\mathrm{Re}(\mathbf{G}\mathbf{G}^{\mathrm{H}})$, Q reaches its maximum. Thus, the eigenvector $\mathbf{v}$ can be used to obtain the Jacobi rotations angle θ, ϕ, and $\mathbf{g}(i,j,\theta,\phi)$ in each iterative calculation [33].

Finally, by a set of Jacobi rotations on the matrices $\{\mathbf{D}_{\mathbf{XX}}(t_k,f_k)^{(i,j)} | k = 1,2,\ldots,K\}$, the joint diagonalization can be realized, and $\mathbf{A}(\theta)$ is the product of all of the rotation matrices. When the iterative convergence is reached, $\mathbf{D}_{\mathbf{SS}}(t_k,f_k)$ in the final step is just the optimization diagonalization matrix. Because $\mathbf{A}(\theta)$ includes all of the DOA information of the impinging signal, $\mathbf{A}(\theta)$ and $\mathbf{D}_{\mathbf{SS}}(t_k,f_k)$ can be used to estimate DOA.

The joint eigenvalue estimation is then

$$\lambda_l = \frac{1}{K}\sum_{k=1}^{K} |\mathbf{D}_{\mathbf{SS}}(t_k,f_k)^{(l,l)}| \qquad (l = 1,2,\ldots,N) \tag{31}$$

Thus, the STFD-based MVDR spatial spectrum based on joint diagonalization using Jacobi rotations can be defined as

$$P_{MVDR}^{TF-JD}(\theta) = \frac{1}{\mathbf{a}^H(\theta)\sum_{l=1}^{N}(\frac{1}{\lambda_l}\mathbf{A}_l(\theta)\mathbf{A}_l^H(\theta))\mathbf{a}(\theta)} \tag{32}$$

where $\mathbf{A}_l(\theta)$ is the l-th column of $\mathbf{A}(\theta)$, which corresponds to the l-th eigenvalue λ_l.

In summary, a procedure to implement our proposed algorithm (or get the solution) is summarized as follows:

(1) Construct the STFD matrix $\mathbf{D_{xx}}(t,f)$ from the array data samples $\mathbf{X}(t)$.
(2) Form K matrices $\mathbf{D_{xx}}(t_k,f_k)$ $(k = 1,2,3,\ldots,K)$ by selecting a fixed set of (t_k,f_k) points, $k = 1,2,3,\ldots,K$.
(3) According to the Jacobis method, the array manifold matrix $\mathbf{A}(\theta)$ is obtained as the joint diagonalizer of the set $\{\mathbf{D_{xx}}(t_k,f_k)|k = 1,2,3,\ldots,K\}$. In addition, when the iterative convergence is reached, the optimization diagonalization matrix $\mathbf{D_{ss}}(t_k,f_k)$ is also obtained in the final step.
(4) The joint eigenvalues are then estimated as $\lambda_l = \frac{1}{K}\sum_{k=1}^{K}|\mathbf{D_{ss}}(t_k,f_k)^{(l,l)}|(l = 1,2,\ldots,N)$ according to Eq. (31).
(5) Finally, the STFDs-based MVDR spatial spectrum based on joint diagonalization using Jacobi rotations is estimated as $P_{MVDR}^{TF-JD}(\theta) = \frac{1}{\mathbf{a}^H(\theta)\sum_{l=1}^{N}(\frac{1}{\lambda_l}\mathbf{A}_l(\theta)\mathbf{A}_l^H(\theta))\mathbf{a}(\theta)}$ according to Eq. (32).

4. Numerical results using synthetic data

In this section, we present several numerical results for the algorithms mentioned above. First, we compare the spatial spectrum for one single source, followed by two closely spaced sources that are strongly correlated (coherent signals). Finally, we discuss and present results on the performance analysis including DOA estimation bias (DEB) and peak-to-sidelobe ratio (PSR). In the following, the array Signal-to-Noise Ratio (SNR) for a single snapshot is defined in decibels

$$\mathrm{SNR} = 20\log_{10}\left(\frac{\|\mathbf{A}(\theta)\mathbf{S}(t)\|_2}{\|\mathbf{N}(t)\|_2}\right) \tag{33}$$

where $\|\mathbf{N}(t)\|_2$ represents the noise l_2-norm and $\|\mathbf{A}(\theta)\mathbf{S}(t)\|_2$ represents the signal l_2-norm. For convenience, we refer to an algorithm based on STFD as the "STFD-algorithm", e.g., CBF based on STFD is

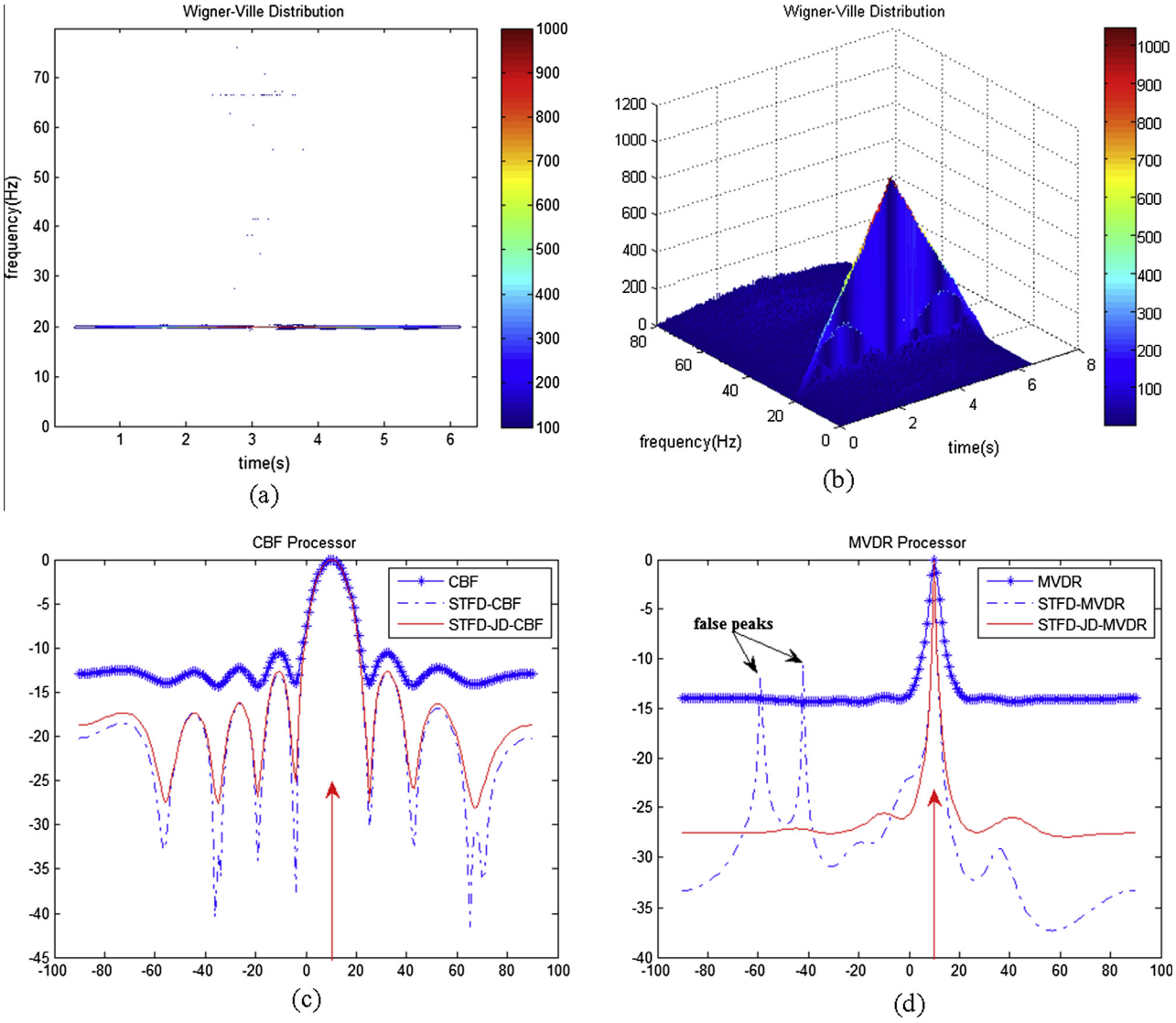

Fig. 2. Numerical results from a single source at 10°. (a) Wigner-Ville Distribution (top view); (b) Wigner-Ville Distribution (three dimensions); (c) Spatial spectrum comparison among CBF, STFD-CBF, and STFD-JD-CBF; (d) Spatial spectrum comparison among MVDR, STFD- MVDR, and STFD-JD- MVDR.

called "STFD-CBF". Similarly, we call an algorithm based on STFD using joint diagonalization as the "STFD-JD-algorithm", e.g., MVDR based on STFD using joint diagonalization is called "STFD-JD-MVDR".

4.1. Spatial spectrum for a single source

Consider a uniform linear array with eight omni-directional sensors and half-wavelength sensor spacing. A single narrowband source signal in the far field impinges on the array from DOA 10°. The signal frequency is 20 Hz, the total number of snapshots is 1024, and the SNR is 5 dB. The numerical results under these conditions are shown in Fig. 2.

Fig. 2(a) and (b) are the Wigner-Ville Distributions, which indicate the time-frequency structure of the signal. For example, in Fig. 2(a), the narrow striation clearly indicates that the arrival has only one narrowband frequency, 20 Hz. Fig. 2(c) compares the spatial spectra obtained by CBF, STFD-CBF, and STFD-JD-CBF. We observe that STFDs-based CBF methods, such as STFD-CBF and STFD-JD-CBF, have lower sidelobes than the conventional CBF method. Fig. 2(d) compares the spatial spectra obtained by MVDR, STFD-MVDR, and STFD-JD-MVDR. We can clearly see that both STFD-MVDR and STFD-JD-MVDR have narrower peaks than MVDR. However, it is also noteworthy that the spatial spectrum obtained by STFD-MVDR has notable false peaks as indicated by the black arrows. The numerical results show the robustness of our proposed method of STFD-JD-MVDR compared to other algorithms.

4.2. Spatial spectrum for closely spaced coherent sources

To illustrate the power of our methodology, we further keep the above simulation condition unchanged, except two coherent sources from distinct DOAs, 3° and 10° respectively, and the SNR is 10 dB. Unfortunately, the strong correlation between the two coherent signals will decay the rank of the data covariance matrix $\mathbf{R_{xx}}$ and the data STFDs matrix $\mathbf{D_{xx}}(t,f)$, so the forward and backward spatial smoothing method for decorrelation is adopted [26,34].The numerical results are shown in Fig. 3.

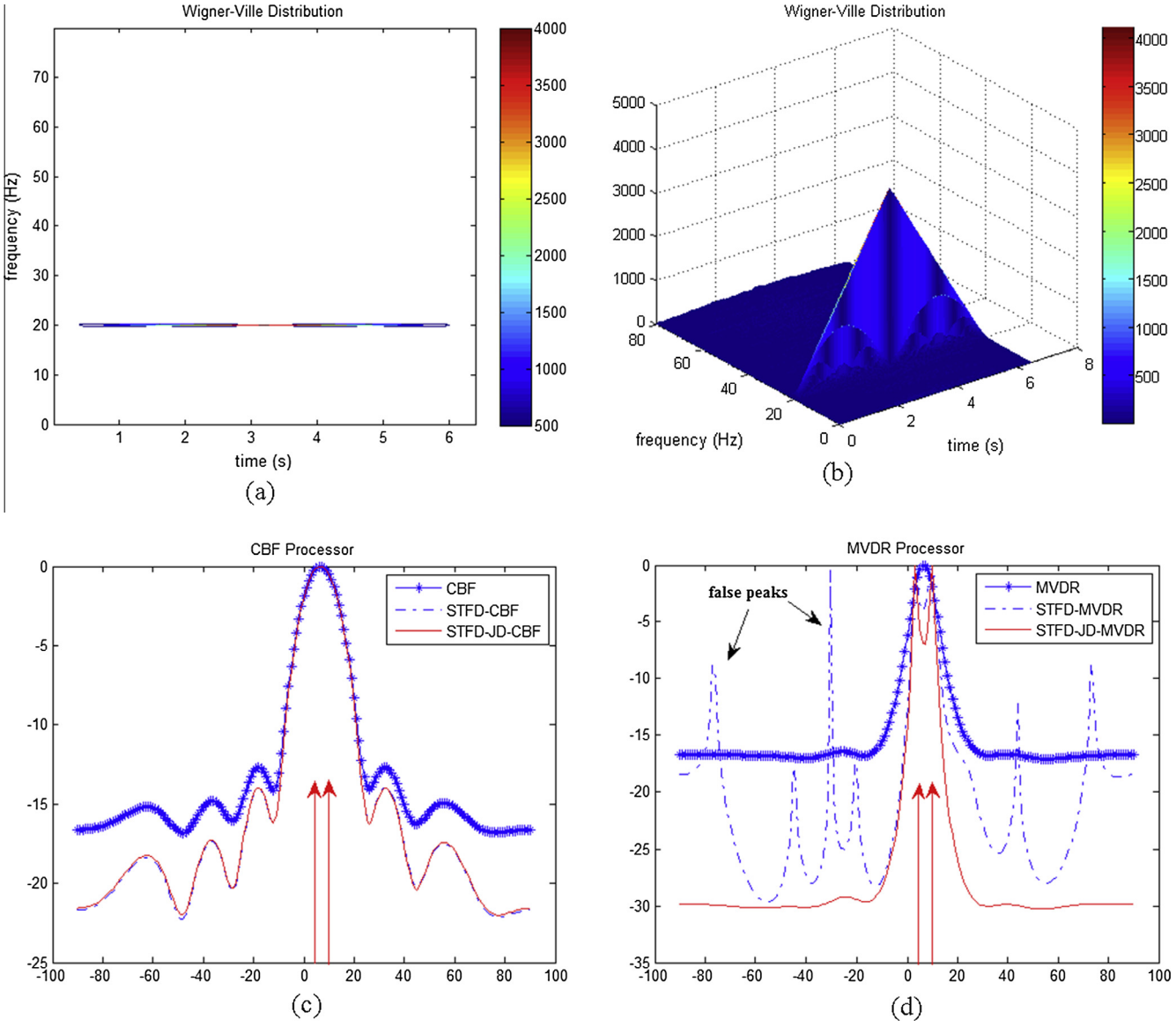

Fig. 3. Numerical results from coherent sources at 3° and 10°. (a) Wigner-Ville Distribution (top view); (b) Wigner-Ville Distribution (three dimension); (c) Spatial spectrum comparison among CBF, STFD-CBF, and STFD-JD-CBF; (d) Spatial spectrum comparison among MVDR, STFD- MVDR, and STFD-JD- MVDR.

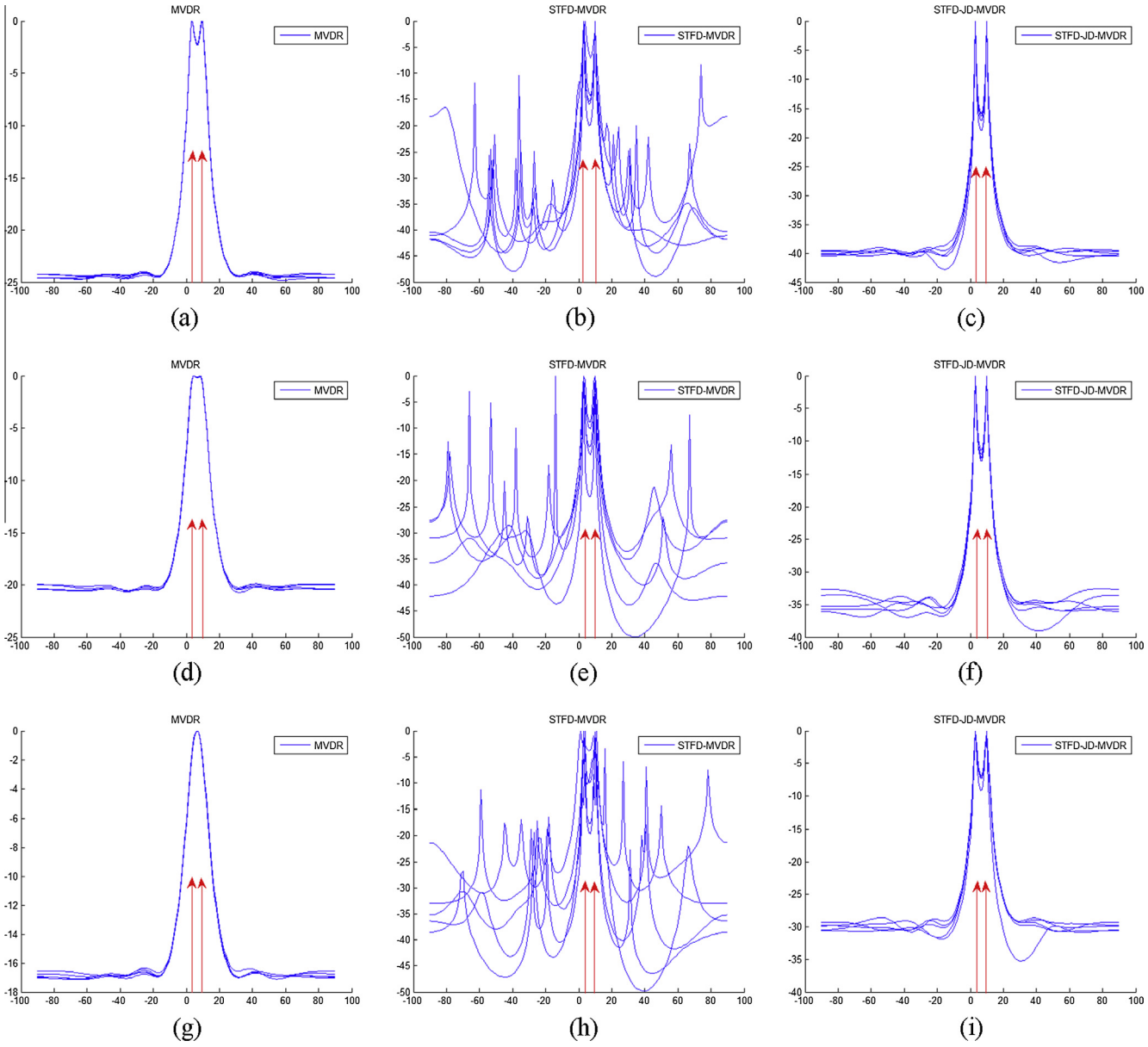

Fig. 4. Numerical results from coherent sources at 3° and 10°. (a) MVDR SNR = 20 dB; (b) STFD-MVDR SNR = 20 dB; (c) STFD-JD-MVDR SNR = 20 dB; (d) MVDR SNR = 15 dB; (e) STFD-MVDR SNR = 15 dB; (f) STFD-JD-MVDR SNR = 15 dB; (g) MVDR SNR = 10 dB; (h) STFD-MVDR SNR = 10 dB; (i) STFD-JD-MVDR SNR = 10 dB.

Fig. 3(a) and (b) are the Wigner-Ville Distributions that reveal the time-frequency information of the signal. As we have already noted, because the two signals are coherent, we cannot distinguish the two distinct DOAs in the time-frequency plans as shown in Fig. 3(a) and (b). In Fig. 3(c), due to the inherent Rayleigh resolution limit of the CBF processor, all of CBF, STFD-CBF, and STFD-JD-CBF cannot resolve the two sources, and there is only one broad peak in each spatial spectrum. Fig. 3(d) compares the spatial spectra obtained by MVDR, STFD- MVDR, and STFD-JD-MVDR, and we observe that both STFD-MVDR and STFD-JD-MVDR have two separated spatial spectrum peaks and can resolve the two closely spaced sources, while conventional MVDR cannot. However, there exist some strong false peaks as indicated by the black arrows in the spatial spectrum of STFD-MVDR, which will submerse the peaks corresponding to the true sources. Thus, under the challenging scenario of more closely spaced coherent sources, STFD-JD-MVDR has higher resolution and lower sidelobes than MVDR and STFD-MVDR.

4.3. Spatial spectrum under different SNRs

The numerical results that we just described in Section 4.2 are under a fixed SNR condition, and the spatial spectrum curve for each algorithm is plotted only once. Now, we illustrate the superior performance by superposing the spatial spectrum curves multiple times under different SNRs.

The simulation condition is similar to the above in Section 4.2, except SNR is 20 dB, 15 dB, and 10 dB. Under this condition, the algorithms based on the CBF processor cannot resolve the two closely spaced sources, so there is no need to present their numerical results. Thus, we only present the numerical results obtained by the algorithms based on the MVDR processor, as shown in Fig. 4.

We can see from Fig. 4 that the performance of each algorithm suffers a slight degeneration as the SNR decreases. For example, MVDR can no longer separate the two sources when the SNR changes from 20 dB to 10 dB. However, it is noted that under the same SNR condition, STFD-JD-MVDR always has higher peaks and

lower sidelobes than the others especially under low SNR. These numerical results indicate that STFD-JD-MVDR outperforms MVDR and STFD-MVDR under different SNRs.

4.4. Statistical performance analysis

Thus far, we have shown the spatial spectrum plots resolving closely spaced coherent sources. We now, from a statistical point of view, investigate the performance of the above-mentioned algorithms more closely by considering DOA estimation with varying SNRs. The DOA estimation performance is specified by the DOA estimation bias (DEB) and peak-to-sidelobe ratio (PSR), where the DEB is defined as the Euclidean distance

$$\mathrm{DEB} = \sqrt{\left(\hat{\theta} - \theta_0\right)^2} \tag{34}$$

where $\hat{\theta}$ and θ_0 respectively represent the estimated DOA and the true DOA. Alternately, the PSR is defined as the ratio

$$\mathrm{PSR} = 10\log_{10}\left(\frac{\mathrm{P_{peak}}}{\mathrm{P_{max-sidelobe}}}\right) \tag{35}$$

where $\mathrm{P_{peak}}$ and $\mathrm{P_{max-sidelobe}}$ respectively represent the power of the highest peak and the power of the maximum sidelobe in the spatial spectrum curve.

The simulation condition is the same as in Section 4.1, except the SNR changes from 10 dB to 20 dB, and the number of Monte Carlo trials is 50 (each point in the plot is the average of 50 trials). The numerical results by the algorithms based on the CBF processor and the algorithms based on the MVDR processor are, respectively, shown in Figs. 5 and 6.

It is noted from Figs. 5(a) and 6(a) that the DEBs for all of the algorithms are nearly equal to zero, so the DOA estimation accu-

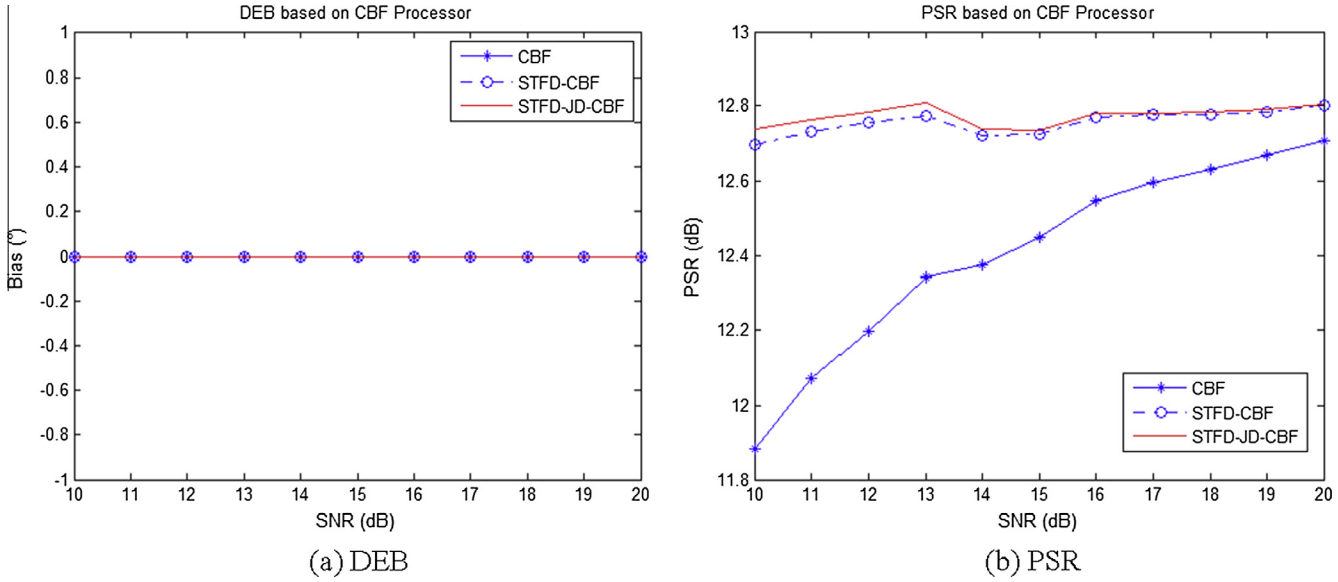

Fig. 5. Numerical results from the algorithms based on the CBF processor.

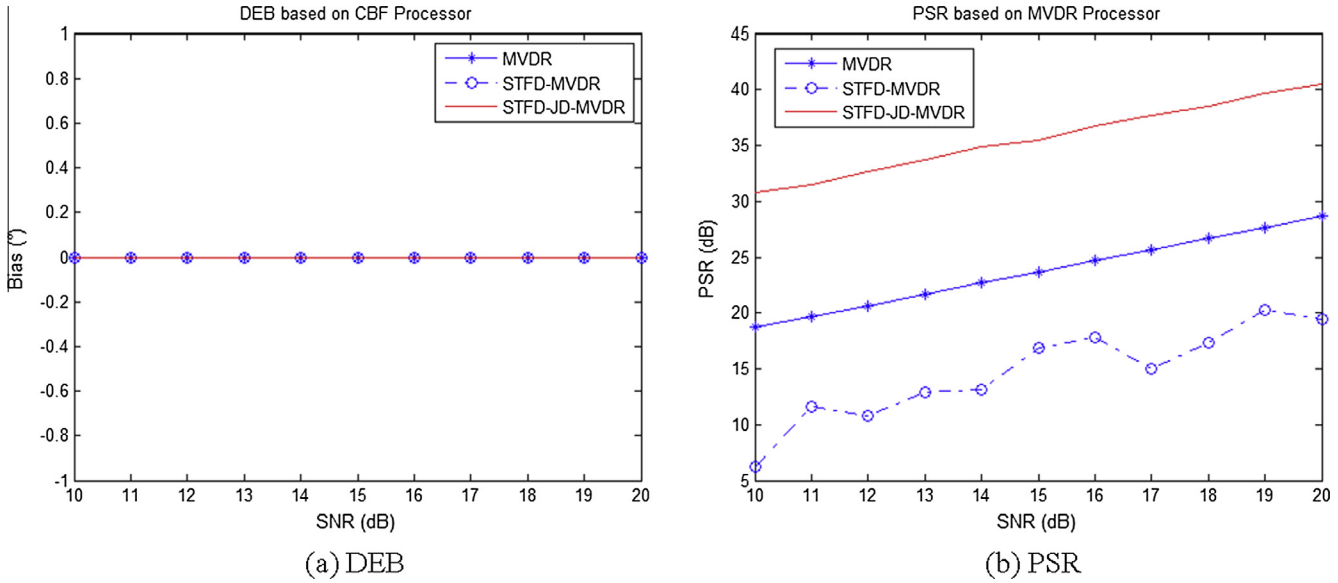

Fig. 6. Numerical results from the algorithms based on the MVDR processor.

racy of STFD-JD-MVDR or STFD-JD-CBF remains comparable to other algorithms. Figs. 5(b) and 6(b) compare the PSRs versus the SNRs. It can be seen that the PSRs from all of the algorithms increase as the SNR increases; however, STFD-JD-MVDR has the highest PSR at all times, especially in the low-SNR case. Thus, this numerical simulation illustrates the superior performance of our proposed algorithm STFD-JD-MVDR compared to other algorithms such as MVDR and STFD-MVDR.

5. Conclusion

A super-resolution DOA estimation approach based on joint diagonalization using Jacobi rotations, which can efficiently combine all of the relevant STFD points, has been proposed in this paper. In addition, the spatial spectrum formulation for STFDs-based MVDR based on joint diagonalization using Jacobi rotations is also derived. The conclusion that can be drawn from the computer simulation results is that our proposed method not only can efficiently address coherent signals but also has higher spatial spectrum peaks and lower sidelobes, especially in the low-SNR case, compared to existing techniques.

Acknowledgments

This work was supported by the Fundamental Research Funds for the Central Universities of Ministry of Education of China (Grant No. HEUCF160501), the National Natural Science Foundation of China (Grant No. 11674074), the Fund for Young Fostering Talents of the Higher Education Institutions in Heilongjiang Province in 2015 (Grant No. UNPYSCT-2015101) and the Postdoctoral Science Foundation of Heilongjiang Province (Grant Nos. LBH-Q15026 and LBH-Z15045).

References

[1] Van Trees HL. Optimum array processing. New York: Wiley; 2002.
[2] Tuncer E, Friedlander B. Classical and modern direction-of-arrival estimation. New York: Elsevier; 2009.
[3] Shi J, Yang DS, Shi SG. Robust localization and identification method of moving sound sources based on worst-case performance optimization. Acta Phys Sin 2011;60(6):064301.
[4] Shi J, Yang DS, Shi SG. Experimental research on cylindrical focused beamforming localization method of moving sound sources based on vector sensor array. Acta Phys Sin 2012;61(12):124302.
[5] Shi J, Yang DS, Shi SG. A robust localization and identification method of noise sources using second-order cone programming. J Harbin Eng Univ 2011;32 (12):1549–55. http://dx.doi.org/10.3969/j.issn.1006-7043.2011.12.005.
[6] Shi J, Yang DS, Shi SG. Near-field source localization algorithm based on the combination array. Acta Electron Sin 2011;39(6):1231–7.
[7] Belouchrani A, Amin MG. Blind source separation based on time-frequency signal representations. IEEE Trans Signal Process 1998;46(11):2888–97. http://dx.doi.org/10.1109/78.726803.
[8] Flandrin P, Amin M, McLaughlin S, Torrsani B. Time-frequency analysis and applications. IEEE Signal Process Mag 2013;30(6):19–20. http://dx.doi.org/10.1109/MSP.2013.2270229.
[9] Cohen L. Time-frequency analysis. New Jersey: Prentice Hall; 1995.
[10] Gao R, Yan R. Wavelets: theory and applications for manufacturing. New York: Springer-Verlag; 2011.
[11] Guo J, Zeng X, She Z. Blind source separation based on high-resolution time-frequency distributions. Comput Electr Eng 2012;38(1):175–84. http://dx.doi.org/10.1016/j.compeleceng.2011.12.002.
[12] Ma N, Goh JT. Ambiguity-function-based techniques to estimate doa of broadband chirp signals. IEEE Trans Signal Process 2006;54(5):1826–39. http://dx.doi.org/10.1109/TSP.2006.871977.
[13] Zhang Y, Amin MG, Himed B. Direction-of-arrival estimation of nonstationary signals exploiting signal characteristics. In: Int. conf. inf. sci., signal process. appl.. ISSPA; 2012. p. 1223–8. http://dx.doi.org/10.1109/ISSPA.2012.6310479.
[14] Belouchrani A, Amin MG. Time-frequency music. IEEE Signal Process Lett 1999;6(5):109–10. http://dx.doi.org/10.1109/97.755429.
[15] Gershman AB, Amin MG. Coherent wideband doa estimation of multiple fm signals using spatial time-frequency distributions. In: ICASSP IEEE int. conf. acoust speech signal process proc.. p. 3065–8.
[16] Gershman A, Amin MG. Wideband direction-of-arrival estimation of multiple chirp signals using spatial time-frequency distributions. IEEE Signal Process Lett 2000;7(6):152–5. http://dx.doi.org/10.1109/97.844636.
[17] Zhang Y, Mu W, Amin MG. Subspace analysis of spatial time-frequency distribution matrices. IEEE Trans Signal Process 2001;49(4):747–59. http://dx.doi.org/10.1109/78.912919.
[18] Ghofrani S. Matching pursuit decomposition for high-resolution direction of arrival. Multidimens Syst Signal Process 2015;26(3):693–716. http://dx.doi.org/10.1007/s11045-013-0266-z.
[19] Ghofrani S. Matching pursuit for direction of arrival estimation in the presence of gaussian noise and impulsive noise. IET Signal Process 2014;8(5):540–51. http://dx.doi.org/10.1049/iet-spr.2013.0286.
[20] Sharif W, Muma M, Zoubir AM. Robustness analysis of spatial time-frequency distributions based on the influence function. IEEE Trans Signal Process 2013;61(8):1958–71. http://dx.doi.org/10.1109/TSP.2013.2246155.
[21] Sharif W, Chakhchoukh Y. Robust spatial time-frequency distribution matrix estimation with application to direction-of-arrival estimation. Signal Process 2011;91(11):2630–8. http://dx.doi.org/10.1016/j.sigpro.2011.05.022.
[22] Khodja M, Belouchrani A, Abed-Meraim K. Performance analysis for time-frequency music algorithm in presence of both additive noise and array calibration errors. EURASIP J Adv Signal Process 2012(1).
[23] Mansour EB, Gervaise C, Khenchaf A. Contributions to passive acoustic oceanic tomography-inversion algorithms based on time frequency space representation for multiple hydrophones processing. In: Oceans 2005 - Europe. p. 919–23. http://dx.doi.org/10.1109/OCEANSE.2005.1513179.
[24] Sabra KG. Single snapshot spatial array processing using time-frequency distributions. Proceedings of meetings on acoustics, vol. 19. http://dx.doi.org/10.1121/1.4800861.
[25] Sabra KG, Anderson SD. Subspace array processing using spatial time-frequency distributions: applications for denoising structural echoes of elastic targets. J Acoust Soc Am 2014;135(5):2821–35. http://dx.doi.org/10.1121/1.4871183.
[26] Krim H, Viberg M. Two decades of array signal processing research. IEEE Signal Process Mag 1996;13(4):67–94. http://dx.doi.org/10.1109/79.526899.
[27] Belouchrani A, Amin MG, Thirion-moreau N, Zhang YD. Source separation and localization using time-frequency distributions: an overview. IEEE Signal Process Mag 2013;30(6):97–107. http://dx.doi.org/10.1109/MSP.2013.2265315.
[28] Zhang XD. Matrix analysis and applications. Bei Jing: Tsinghua University Press; 2004.
[29] Song HY, Piao SC. Doa estimation method based on orthogonal joint diagonalization of high-order cumulant. J Electron Inform Technol 2010;32 (4):967–72. http://dx.doi.org/10.3724/SP.J.1146.2008.01176.
[30] Cardoso JF, Souloumiac A. Jacobi angles for simultaneous diagonalization. SIAM J Martix Anal Appl 1996;17(1):1–3.
[31] Golub GH, Van Loan CF. Matrix computations. London: The Johns Hopkins University Press; 1996.
[32] Belouchrani A, Abed-Meraim K, Cardoso JF, Moulines E. Blind source separation technique using second-order statistics. IEEE Trans Signal Process 1997;45(2):434–44.
[33] Song HY, Piao SC. Two new doa estimation methods based on orthogonal joint diagonalization. In: IEEE conf. ind. electron. appl.. ICIEA; 2009. p. 1110–4. http://dx.doi.org/10.1109/ICIEA.2009.5138374.
[34] Wolfram P. Spatial smoothing for localized correlated sources – its effect on different localization methods in the nearfield. Appl Acoust 2011;72 (11):873–83. http://dx.doi.org/10.1016/j.apacoust.2011.05.011.